Probing Excited-State Electron Transfer by Resonance Stark Spectroscopy: 3. Theoretical Foundations and Practical Applications

Thomas P. Treynor and Steven G. Boxer*

Department of Chemistry, Stanford University, Stanford, California 94305-5080

Received: March 5, 2004; In Final Form: May 21, 2004

Resonance Stark effects are nonclassical Stark effects associated with excited-state charge-transfer processes. The theory of resonance Stark effects developed in Part 2 of this series is generalized in a number of respects. The equations are modified to allow for violations of the Condon approximation and to allow for inhomogeneous contributions to absorption and Stark line shapes. A distinction is drawn between higher-order Stark spectra and Stark spectra that depend on integral powers of the applied electric field, and it is shown how this can affect analyses of resonance Stark effects. Covariances among the parameters that are used to fit absorption spectra and resonance Stark effects are described, and their impact is described in the context of the data for photosynthetic reaction centers that is presented and analyzed further in Part 4 (Treynor, T. P.; Yoshina-Ishii, C.; Boxer, S. G. *J. Phys. Chem. B,* **2004**, *108,* 13523. Equations are derived that provide a mapping between the parameters used in Marcus theory and those used in radiationless transition theory.

Resonance Stark spectroscopy is a new spectroscopic technique that can provide information on many factors that affect excited-state charge-transfer reactions. In Part 1, we described the discovery of the resonance Stark effect (RSE) in the course of studies of the higher-order Stark (HOS) spectra of photosynthetic reaction centers (RCs).[1] RSEs can be readily distinguished from classical Stark effects[2] due to their different line shapes and relative intensities. In Part 2, a theoretical model was developed showing that the resonance Stark effect is a natural consequence of the physics of photoinduced charge-transfer reactions in applied electric fields and should therefore be useful for studying excited-state charge-transfer dynamics.[3] Additionally it was shown that for reasonable values of charge-transfer parameters, the wide range of intensities and unusual HOS line shapes observed for reaction center variants could be captured. In this paper, we develop the theory further with particular attention to underlying assumptions and the analysis of data. We also consider how experimental factors can affect the analysis and conclude with a prescription for a more quantitative analysis of resonance Stark spectra, which is applied in Part 4 to a series of reaction center variants.[4]

To develop the theory of the resonance Stark effect such that it connects directly to the more familiar treatments of electron transfer,[5] we must establish a conceptual framework and notation that emphasizes these connections and eliminates some subtle sources of confusion among these treatments. These treatments invariably calculate electron-transfer kinetics as a function of two factors: the geometry of the initial and final state potential energy surfaces and the coupling between those surfaces. For example, the rate of a thermally activated electron-transfer reaction, k_{et}, is typically expressed as

$$k_{et} = \frac{2\pi}{\hbar} V_0^{\,2} \mathrm{FC} \qquad (1)$$

where V_0 is the electronic coupling and FC is the Franck−Condon factor.[5,6] This product reflects a separation of the electronic and nuclear coordinates of the initial and final state wave functions, which is achieved by imposing both the Born−Oppenheimer and Condon approximations.

Eq 1 may look simple, but even the simplest theories of electron transfer require two additional parameters to determine FC.[5] Generally these two parameters are the driving force, $\Delta\bar{\nu}$, and the reorganization energy, λ, as illustrated in Figure 1A. Although the notation that we have chosen suggests that these are spectroscopically observable internal energies, for reasons that will become more evident below, these symbols could just as well represent standard free energies. Complicating things further, this simplest description hinges upon the assumptions that both the initial and final state surfaces are parabolic and have the same curvature. The result of this treatment of electron transfer, credited to Marcus,[7] is that $\Delta\bar{\nu}$ and λ determine the free energy of the transition state, $\bar{\nu}^{\ddagger}$, such that k_{et} can be calculated using an Arrhenius expression that resembles eq 1:

$$k_{et} = \frac{2V_0^{\,2}}{h}\sqrt{\frac{\pi^3}{\lambda k_B T}}\exp\left[\frac{-(\Delta\bar{\nu}+\lambda)^2}{4\lambda k_B T}\right] \qquad (2)$$

In some experiments $\Delta\bar{\nu}$ can be measured under the same conditions as k_{et}, but even in these optimal circumstances, experimentalists are unable to separate the contributions of V_0 and λ to k_{et}. They are forced to vary the conditions of the electron-transfer reactions in one way or another to tease apart these contributions from the coupling and the reaction surface geometry by increasing the dimensionality of the data sets. For example, it is common to measure rates at many different temperatures, although $\Delta\bar{\nu}$, λ, and V_0 may themselves be functions of temperature. Likewise, $\Delta\bar{\nu}$ can be perturbed by ligand substitution, functional derivatization, or changes to an organized host matrix such as a protein, yet it is usually assumed that V_0 and λ are *not* perturbed when the kinetic data are analyzed.

The Hush treatment of charge transfer demonstrated that one could separate the influences of V_0 and the reaction surface

* To whom correspondence should be addressed. Phone: (650)723-4482. Fax: (650)723-4817. E-mail: Sboxer@stanford.edu.

10.1021/jp048988x CCC: $27.50
Published on Web 08/07/2004

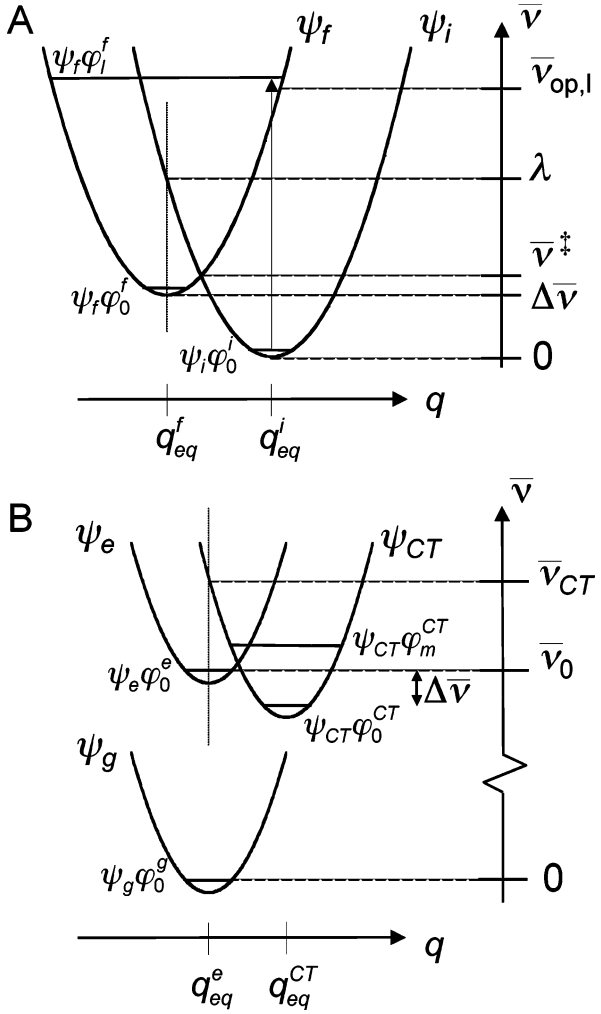

Figure 1. Three different kinds of charge-transfer processes. Panel A depicts the two potential energy surfaces involved in both thermally activated electron transfer and the direct optical excitation of charge transfer; Panel B depicts the three surfaces involved in excited-state charge transfer. If Panel A is used to describe thermally activated electron transfer, the vertical axis should be considered a standard free energy axis as opposed to a spectroscopic energy axis. The parameters q_{eq}^{i}, q_{eq}^{f}, q_{eq}^{e}, and q_{eq}^{CT} are the equilibrium nuclear configurations of the initial, final, excited, and charge-transfer electronic states, denoted ψ_i, ψ_f, ψ_e, and ψ_{CT}, respectively. The ground electronic state for the case of excited-state charge transfer, denoted ψ_g, is drawn as having the same equilibrium nuclear configuration as ψ_e to emphasize the horizontal displacement between ψ_e and ψ_{CT}. Other parameters are defined in the text.

geometry upon an electron-transfer event in a single experiment if the observable were a spectrum instead of a rate constant.[8] Such charge-transfer spectra arise when the coupling between the ground state and an otherwise dark charge-transfer state permits the direct optical excitation of the electron transfer. In these situations, again illustrated in Figure 1A, V_0 can be determined from the integrated intensity of the charge-transfer band and an estimate of the distance of charge transfer. When the Born−Oppenheimer and Condon approximations are imposed in a weak coupling limit, this oscillator strength is distributed into a vibronic progression, FC_{0l}^{vert}, with intensities proportional to the square of the overlap integral between the vibrational wave functions of the initial and final states:

$$FC_{0l}^{vert} = |\langle\varphi_0^i|\varphi_l^f\rangle|^2 \tag{3}$$

where φ_0^i denotes the ground vibrational state of the initial electronic state ψ_i, and φ_l^f denotes the lth vibrational state of the final electronic state ψ_f. The superscript vert refers to the fact that the charge-transfer transition is made vertically, along the energy axis in Figure 1A. Like FC in eq 1, FC_{0l}^{vert} is also a Franck−Condon factor. The two Franck−Condon factors are *not* identical, although they embody identical assumptions. Whereas FC is a single value calculated using the transition-state energy, $\bar{\nu}^\ddagger$, FC_{0l}^{vert} is multivalued with its largest values corresponding to states with energies necessarily larger than $\bar{\nu}^\ddagger$. The values of these FC_{0l}^{vert}, once culled from a spectrum, can be used to determine $\Delta\bar{\nu}$ and λ. Like RSEs, the Stark effects of these charge-transfer bands may be nonclassical in nature.[9,10]

Spectral analysis can also yield V_0 and a description of the reaction surface geometry for excited-state charge-transfer reactions, where the charge-transfer state is coupled not to the ground state but rather to an excited state prepared by the absorption of a photon. This situation is illustrated in Figure 1B. Drawn from radiationless transition theory,[11] the appropriate Franck−Condon factor is one that describes a *horizontal* transition between the surfaces corresponding to the excited and charge-transfer states:

$$FC_{0m}^{horiz} = |\langle\varphi_0^e|\varphi_m^{CT}\rangle|^2 \tag{4}$$

where φ_0^e denotes the ground vibrational state of the excited electronic state ψ_e, and φ_m^{CT} denotes the mth vibrational state of the charge transfer state ψ_{CT}. This is a *third* definition for a Franck−Condon factor used to describe a third kind of charge-transfer process. Nevertheless, this third definition embodies identical assumptions as the two before. This third kind of charge-transfer process is most sensitive to a region of the reaction surface geometry that is typically distinct from either of the regions that most strongly influence thermally activated electron-transfer rates or charge-transfer absorption bands: the FC_{0m}^{horiz} that have the largest effect on the absorption spectrum are generally those that are quasidegenerate with $\psi_e\varphi_0^e$.

The distinction between vertical and horizontal transitions makes a tremendous difference on the appearance and interpretation of the optical spectra. For one, the value of V_0 does not influence the integrated absorption intensity when the charge-transfer process is an excited-state horizontal transition. Second, in the weak coupling limit the width of a charge-transfer absorption band is sensitive only to the *horizontal* displacement between the initial and final state surfaces; in contrast, the width of an absorption band coupled to an excited-state horizontal transition is sensitive both to horizontal and to vertical displacements of the ψ_{CT} surface. Moreover, in the limit where the vibrational wave functions on the ψ_{CT} surface are densely packed and the discrete FC_{0m}^{horiz} are replaced with the continuous Franck−Condon weighted density of states, $\rho FC(\bar{\nu})$, the contribution to the homogeneous absorption line width from electron transfer, Γ_{et}, is related to k_{et} according to

$$\Gamma_{et} = k_{et}/2\pi \tag{5}$$

in accord with the limiting equality of Heisenberg's time−energy uncertainty relationship.[12] The contribution to the absorption line width from a vertical charge-transfer transition cannot be interpreted this way.

Thus, if Γ_{et} dominates the contributions to the absorption line width, then k_{et} can be estimated directly from that line width. Moreover, when this line width is taken together with the higher moments of the line shape, one has enough information to determine V_0, as well as the mean, $\bar{\nu}_{CT}$, and higher moments of

the normalized distribution $\rho_{FC}(\bar{\nu})$, the very parameters that are convolved using Fermi's golden rule to yield the value of k_{et} in an expression reminiscent of eq 1:

$$k_{et} = 2\pi^2 V_0^{\,2} \rho_{FC}(\bar{\nu}_0) \tag{6}$$

where $\bar{\nu}_0$ is the vertical displacement between the potential energy surfaces corresponding to ψ_e and the ground electronic state, denoted ψ_g. However, there are few examples in the condensed phase where an excited-state charge-transfer process is the dominant source of line broadening.[13]

Resonance Stark spectroscopy makes it possible to determine V_0, $\bar{\nu}_0 - \bar{\nu}_{CT}$, and the full width at half-maximum of $\rho_{FC}(\bar{\nu})$, denoted Δ_{CT}, even when the contribution of charge transfer to the total line width is slight.[3] The change in an absorption spectrum due to an applied electric field, $\vec{F}$, is called a Stark spectrum. Resonance Stark spectroscopy utilizes the interaction of $\vec{F}$ with the difference between the electric dipole moments of the ψ_e and ψ_{CT} surfaces, $\Delta\vec{\mu}_{CT}$, to characterize the coupling and the reaction surface geometry in the absence of the field by changing the vertical displacement of these surfaces with respect to one another:

$$\bar{\nu}_{CT}(\vec{F}) = \bar{\nu}_{CT} - \vec{F}\cdot f\Delta\vec{\mu}_{CT} \tag{7}$$

The parameter f in eq 7 is the scalar approximation to the local field correction tensor. This tensor is intended to account for a possible difference between $\vec{F}$, the externally applied field, and $\vec{F}_{int}$, the internal field at the position of a chromophore: $\vec{F}_{int} = f\cdot\vec{F}$. It is generally believed that for most frozen organic or aqueous glasses the value of f should be between 1.0 and 1.3.[2,14]

If it were assumed that the electric field changes only the absorption *energy* and *intensity* and not the absorption *line shape*, one would analyze the Stark spectrum

$$\Delta A(F) = A(F\neq 0) - A(F=0) \tag{8}$$

with equations first derived by Liptay.[15,16] These equations include the interactions of the field with the dipole moments and polarizabilities of the ground and excited electronic states and other electrooptic factors. In the following, we will refer to these Stark effects as classical Stark effects. For most isolated molecules studied to date, this formulation provides an adequate, if not perfect, description of the observed electronic and vibrational Stark spectra.[2] In the case where excited-state electron transfer occurs, however, the electric field will perturb not just the peak shift induced by the coupling of ψ_e to ψ_{CT} but the lifetime broadening as well. This Stark effect is fundamentally different from a classical Stark effect, Liptay's equations cannot describe it at all, and we call it a resonance Stark effect.

Theoretical Foundations

The phenomenological foundation of resonance Stark theory is the same as that of radiationless transition theory, which attempts to explain the irreversible decay of a state under the influence of any nonradiative relaxation mechanism, including charge transfer.[11] This foundation is constructed by analogy to radiative decay by postulating a continuous bath of accepting states to which the initial state is coupled. This analogy is straightforward, for example, when considering autoionization in the gas phase, where an atom excited to a discrete metastable state, ϕ, decays into a continuum of free electron states, denoted by their energies, $\bar{\nu}$. The Hamiltonian for this problem is

$$\begin{aligned} \langle\phi|H|\phi\rangle &= \bar{\nu}_0 \\ \langle\phi|H|\bar{\nu}\rangle &= V(\bar{\nu}) \\ \langle\bar{\nu}|H|\bar{\nu}'\rangle &= \bar{\nu}'\delta(\bar{\nu}' - \bar{\nu}) \end{aligned} \tag{9}$$

and has been diagonalized exactly by Fano.[12] The probability density $|a(\bar{\nu})|^2$ of the state ϕ in the eigenstates, themselves denoted by $\bar{\nu}$, is given by a simple pseudo-Lorentzian expression for any arbitrary form of the off-diagonal matrix elements, $V(\bar{\nu})$:

$$|a(\bar{\nu})|^2 = \frac{|V(\bar{\nu})|^2}{[\bar{\nu} - \bar{\nu}_0 - U(\bar{\nu})]^2 + \pi^2|V(\bar{\nu})|^4} \tag{10}$$

where

$$U(\bar{\nu}) = P\int \mathrm{d}\bar{\nu}' \frac{|V(\bar{\nu}')|^2}{\bar{\nu} - \bar{\nu}'} \tag{11}$$

and P denotes the Cauchy principal value of the integral. $U(\bar{\nu})$, the Hilbert transform of $|V(\bar{\nu})|^2$, is the interaction-induced shift to the absorption spectrum for excitation from the ground state to ϕ, whereas $\pi|V(\bar{\nu})|^2$ is the interaction-induced broadening to this spectrum. In cases where the Condon approximation is applicable, $|V(\bar{\nu})|^2$ can be written as $V_0^2\rho_{FC}(\bar{\nu})$, a product of terms with electronic and vibrational origins, respectively.

In contrast, the analogy with radiative processes is not at all straightforward when considering decay into a bound state, such as ψ_{CT}, the vibrational levels of which are inherently discrete. Our desire to demonstrate the applicability of this analogy stems from the ease with which we can use eq 10 to develop an analytical description for resonance Stark spectra, in which case the states $\psi_e\varphi_0^e$ and $\psi_{CT}\varphi_m^{CT}$ are analogous to the states ϕ and $\bar{\nu}$ in eq 9, respectively. Thus we step back and consider the conditions under which these equations for decay into a continuum can be relevant to decay into a bound state.

Single-Mode Model. We begin by assuming that there is no difference in the equilibrium nuclear configurations of the ψ_g and ψ_e surfaces (as illustrated in Figure 1) such that the only Franck−Condon allowed transition from the ground vibrational state of ψ_g is to the ground vibrational state of ψ_e, provided there is no coupling between ψ_e and ψ_{CT}. We assume also that the difference in the equilibrium nuclear configurations of the ψ_e and ψ_{CT} surfaces is along a single normal vibrational mode, q. With respect to the state $\psi_e\varphi_0^e$, the vibrational states on the ψ_{CT} surface will appear to be effectively continuous in the limit where the couplings between $\psi_e\varphi_0^e$ and the states $\psi_{CT}\varphi_m^{CT}$ nearest in energy are considerably larger than $\bar{\nu}_q$, the vibrational spacing for the mode q. In this limit, the states $\psi_{CT}\varphi_m^{CT}$ are mixed significantly with each other by their mutual interactions with $\psi_e\varphi_0^e$ such that the envelope of the vibronic transition from the ground state is relatively insensitive to the value of $\bar{\nu}_q$. We will refer to this as the single-mode continuum condition:

$$\langle\psi_e\varphi_0^e|H|\psi_{CT}\varphi_m^{CT}\rangle \gg \bar{\nu}_q \tag{12}$$

If the horizontal displacement between the two surfaces (see Figure 1),

$$\Delta = q_{eq}^{CT} - q_{eq}^{e} \tag{13}$$

is zero and the Condon approximation is assumed, then FC_{0m}^{horiz} is $\delta(m)$, and eq 12 can only be satisfied for the single state $\psi_{CT}\varphi_0^{CT}$. Nonzero displacement, also referred to as linear electron−phonon coupling, will broaden this δ function. The

Franck−Condon spectrum is then Poisson-distributed:

$$\mathrm{FC}_{0m}^{\mathrm{horiz}} = \frac{S^m \exp(-S)}{m!} \tag{14}$$

where S is the Huang−Rhys parameter, given by

$$S = \Delta^2/2 \tag{15}$$

When $S \geq 3$, eq 14 resembles a slightly skewed Gaussian with mean equal to S, maximum at $S - (1/2)$, and standard deviation of $\sqrt{S}$. Multiplication of these dimensionless values by $\bar{\nu}_q$ places them onto an energy scale; in particular,

$$\lambda = \bar{\nu}_q S \tag{16}$$

However, whenever the single-mode continuum condition is satisfied, one cannot ignore the presence of higher vibrational states on the ψ_e surface, as is done implicitly in eq 9, because their overlap integrals with the vibrational states on the ψ_{CT} surface are significant as well. As a result, there is a considerable superexchange coupling between vibrational states on the ψ_e surface mediated by their couplings to the $\psi_{CT}\varphi_m^{CT}$ states. Thus one suspects that eq 10 cannot successfully approximate the results from diagonalizing this complete Hamiltonian, and we must consider a different model for the charge-transfer process.

Multiple-Modes Model. We therefore assume that the linear electron−phonon coupling involves displacement along multiple normal vibrational modes, q_j. As suggested by the analysis of the single-mode model, our goal with the multiple-modes model is to show that the mixing among vibrational states on the ψ_e surface is insignificant. If this is true, then we can effectively ignore all but the ground vibrational state on the ψ_e surface by using eq 10 to describe the effect of the coupling between ψ_e and ψ_{CT} on the transition from the ground vibronic state of the system.

When multiple modes are dealt with explicitly, the expression for the Franck−Condon factor becomes

$$\mathrm{FC}_{0\{m_j\}}^{\mathrm{horiz}} = \prod_j |\langle \varphi_0^{e,j} | \varphi_{m_j}^{CT,j} \rangle|^2 \tag{17}$$

where $\varphi_0^{e,j}$ is the ground vibrational wave function along the jth normal mode on the ψ_e surface, and $\varphi_{m_j}^{CT,j}$ is the mth vibrational wave function along the jth normal mode on the ψ_{CT} surface. The simplest treatment of displacement along multiple modes is that introduced by Huang and Rhys to describe vertical transitions.[17] With regard to a sample of N atoms with a number of vibronically coupled modes on the order of N, they made two assumptions: (i) a single mean frequency, $\bar{\nu}_{mean}$, is used to describe each mode, and (ii) the displacement of each mode is on the order of $1/\sqrt{N}$. Sturge et al.[18] argued that a similar model was valid for horizontal transitions influencing the absorption spectra of transition-metal impurities in solids, and we use a similar argument here, one which recognizes the intrinsic dispersion of the vibrational frequencies about $\bar{\nu}_{mean}$, for the case of an excited-state charge-transfer reaction.

Like the single-mode continuum condition, the multiple-modes continuum condition is that the couplings between the ground vibrational state of ψ_e and the vibrational states of ψ_{CT} nearest in energy are larger than the spacing between those states. Whereas this spacing was equal to $\bar{\nu}_q$ in the single-mode model, in the multiple-modes model this spacing rapidly approaches zero as the total vibrational energy of ψ_{CT} increases due to the deviations of the frequencies of many modes from $\bar{\nu}_{mean}$; this spacing decreases because various numbers of vibrational quanta in the different modes can be combined in an increasing number of ways such that the total vibrational energy falls within a given interval. The multiple-modes continuum condition is then equivalent to the statement that the mean number of vibrational quanta gained by crossing from the ψ_e surface to the ψ_{CT} surface is large:

$$\Delta\bar{\nu} \gg \bar{\nu}_{mean} \tag{18}$$

In this limit, the vibrational states on the ψ_{CT} surface are densely packed for all values of $\bar{\nu}$ near $\bar{\nu}_0$. Because displacements are on the order of $1/\sqrt{N}$, the squared vibrational overlap between $\psi_e\varphi_0$ and any *single state* with energy $\bar{\nu}_0$ on the ψ_{CT} surface is on the order of $(1/N)^{\Delta\bar{\nu}/\bar{\nu}_{mean}}$, where the exponent is the mean number of vibrational quanta gained by the horizontal transition from $\psi_e\varphi_0$ to ψ_{CT}. Since the density of vibrational states on the ψ_{CT} surface at energy $\bar{\nu}_0$ is on the order of $N^{\Delta\bar{\nu}/\bar{\nu}_{mean}}$, the vibrational contribution to the mixing of $\psi_e\varphi_0$ with this particular *energy level*, $\rho_{FC}(\bar{\nu}_0)$, is on the order of one.

The vibrational contribution to the ψ_{CT}-mediated mixing between $\psi_e\varphi_0$ and other *states* on the ψ_e surface is a function of the product of two squared vibrational overlap integrals. For the case of one quantum of vibrational excitation (i.e., states with energy $\bar{\nu}_0 + \bar{\nu}_{mean}$), its value is on the order of $(1/N)^{1+(\Delta\bar{\nu}/\bar{\nu}_{mean})} \times (1/N)^{(\Delta\bar{\nu}/\bar{\nu}_{mean})}$. Although the density of vibrational states on the ψ_{CT} surface is roughly $N^{1+(\Delta\bar{\nu}/\bar{\nu}_{mean})}$ at this energy, the density of states on the ψ_e surface is only N. In this way, it can be shown that when eq 18 is satisfied, the vibrational contribution to the ψ_{CT}-mediated mixing between $\psi_e\varphi_0$ and nearby *energy levels* on the ψ_e surface is essentially zero.

As we had hoped, we can ignore all but the ground vibrational state on the ψ_e surface and apply Fano's formula to excited-state charge transfer, a problem of decay into a bound state, provided we have a form for $\rho_{FC}(\bar{\nu})$. Sturge et al. demonstrate that their spectra are fit well using a continuous analogue to eq 14, as justified by Markham for a low-temperature limit ($k_BT \ll \bar{\nu}_{mean}$).[18,19] The form of this equation is determined by replacing m with $\bar{\nu}'/\bar{\nu}_{mean}$, where $\bar{\nu}' = \bar{\nu} - (\bar{\nu}_0 - \Delta\bar{\nu})$, and by replacing $m!$ with $\Gamma[(\bar{\nu}'/\bar{\nu}_{mean}) + 1]$:

$$\rho_{FC}(\bar{\nu}) = \frac{S^{\bar{\nu}'/\bar{\nu}_{mean}} \exp(-S)}{\Gamma[(\bar{\nu}'/\bar{\nu}_{mean}) + 1]} \tag{19}$$

where $S = \sum S_j$, the sum of the Huang−Rhys parameters for displacements along the q_j modes. This continuous version of a Poisson distribution has been referred to as a Pekarian.[18,19] Markham argues that, as temperature is raised, the form of $\rho_{FC}(\bar{\nu})$ evolves from the Pekarian into a Gaussian due to an increasingly significant population of the higher vibrational states on the ψ_g surface.[19] As seen below, the choice of the functional form for $\rho_{FC}(\bar{\nu})$ affects the analyses of RSEs.

A More General Resonance Stark Theory. The derivation of resonance Stark theory in Part 2 assumed that $\rho_{FC}(\bar{\nu})$ was a normalized Gaussian. We will refrain from making this assumption in what follows since Markham has demonstrated that the form of $\rho_{FC}(\bar{\nu})$ may in general lie somewhere on the spectrum from Pekarian to Gaussian. Moreover, violations of the Condon approximation may prevent the decomposition of $|V(\bar{\nu})|^2$ into V_0^2 and $\rho_{FC}(\bar{\nu})$ in the first place. By deriving a more general resonance Stark theory than that presented in Part 2, one might use resonance Stark effects to investigate these details of $V(\bar{\nu})$.

As in Part 2, we begin with the full complex dielectric function:

$$\epsilon(\bar{\nu}) = \frac{1}{\bar{\nu} - \bar{\nu}_0 - U(\bar{\nu}) - i\pi|V(\bar{\nu})|^2 - i\Gamma_0} \tag{20}$$

the absorptive part of which is given by eq 10 when $\Gamma_0 = 0$. The phenomenological broadening term, Γ_0, is inserted to account for any exponential decay mechanisms that are not the electron-transfer reaction of interest, for example, fluorescence, internal conversion, and intersystem crossing, each of which we will treat as independent of the applied electric field, $\vec{F}$.

In the presence of $\vec{F}$, the entire curve

$$W(\bar{\nu}) = U(\bar{\nu}) + i\pi|V(\bar{\nu})|^2 \tag{21}$$

will shift with respect to $\bar{\nu}_0$ according to eq 7. To determine the effect of this shift on the complex dielectric function, we expand $\epsilon(\bar{\nu})$ as a Taylor's series in $\Delta W(\bar{\nu},\vec{F})$ to get

$$\Delta\epsilon(\bar{\nu},\vec{F}) = \epsilon^2(\bar{\nu})\Delta W(\bar{\nu},\vec{F}) + \epsilon^3(\bar{\nu})\Delta W^2(\bar{\nu},\vec{F}) + \epsilon^4(\bar{\nu})\Delta W^3(\bar{\nu},\vec{F}) + ... \tag{22}$$

where we have substituted $(k-1)!\epsilon^k(\bar{\nu})$ for the $(k-1)$th derivative of $\epsilon(\bar{\nu})$ with respect to ΔW. In turn, ΔW can be expanded as a Taylor's series in $\vec{F}\cdot f\Delta\vec{\mu}_{CT}$, such that

$$\Delta W(\bar{\nu},\vec{F}) = W^{(1)}(\bar{\nu})\vec{F}\cdot f\Delta\vec{\mu}_{CT} + \frac{W^{(2)}(\bar{\nu})}{2!}(\vec{F}\cdot f\Delta\vec{\mu}_{CT})^2 + \frac{W^{(3)}(\bar{\nu})}{3!}(\vec{F}\cdot f\Delta\vec{\mu}_{CT})^3 + ... \tag{23}$$

where $W^{(n)}$ is the nth derivative of W with respect to $\bar{\nu}$.

When eqs 22 and 23 are combined, it is clear how the RSE for any single charge-transfer system can be decomposed into terms that depend on the nth power of the projection of $\vec{F}$ onto $\Delta\vec{\mu}_{CT}$. Additionally, the magnitude of the Stark spectrum is proportional to the magnitude of the absorption spectrum, which depends on the square of the projection of the polarization of light, $\hat{e}$, onto the transition moment, $\vec{m}$. An expression for the Stark spectrum of an ensemble will reflect the connection between these two phenomena with terms of the form

$$m^2(Ff\Delta\mu_{CT})^n\langle\cos^2\alpha\cos^n\beta\rangle \tag{24}$$

where α is the angle between $\vec{m}$ and $\hat{e}$, β is the angle between $\vec{F}$ and $\Delta\vec{\mu}_{CT}$, and $\langle ...\rangle$ denotes an average over the distribution of orientations of the charge-transfer systems in the ensemble. The calculation of this orientational average can be simplified by noting that (i) the angle χ between $\vec{F}$ and $\hat{e}$ is fixed in the lab frame (and can be varied experimentally) and (ii) the angle ζ_{CT} between $\Delta\vec{\mu}_{CT}$ and $\vec{m}$ is fixed in the molecular frame (and depends on the intrinsic properties of the charge-transfer system). For an isotropic sample, these two frames take any relative orientation with equal probability, simplifying eq 24 to

$$\begin{cases} \dfrac{m^2(Ff\Delta\mu_{CT})^n}{3(n+1)(n+3)}\left[(n+3) + \dfrac{n}{2}(3\cos^2\chi - 1)(3\cos^2\zeta_{CT} - 1)\right] & \text{for even } n \\ 0 & \text{for odd } n \end{cases} \tag{25}$$

If we let n equal zero, this equation applies to the absorption spectrum itself. For all values of n, this factor contains a divisor of three; thus, comparisons between absorption and Stark spectra would be unchanged if we were to ignore this factor of 3, as was done in Part 2.

In the weak coupling limit, where Γ_0 is large compared to $V(\bar{\nu})$ for all $\bar{\nu}$, the absorptive line shape from eq 20 is Lorentzian. For real systems in the condensed phase, this line shape is often significantly inhomogeneously broadened. $\epsilon(\bar{\nu})$ must then be convolved with an inhomogeneous broadening function, $b(\bar{\nu})$:

$$\epsilon'(\bar{\nu}) = \int_{-\infty}^{\infty} d\bar{\nu}'\, \epsilon(\bar{\nu} - \bar{\nu}')b(\bar{\nu}') \tag{26}$$

If we assume that eq 20 yields the same homogeneous line shape for each value of $\bar{\nu}_0$ across the inhomogeneously broadened band, then we express the Stark spectrum as

$$\Delta A(\bar{\nu},F) = \mathrm{Im}[\Delta\epsilon(\bar{\nu},F)]*b(\bar{\nu}) \tag{27}$$

For a particular choice of Γ_0, the determination of $b(\bar{\nu})$ by deconvolution is unique. Conversely, if one were to impose a restriction on the functional form of $b(\bar{\nu})$ (e.g., a Gaussian with full width at half-maximum equal to Γ_{Gaus}), then there should exist a best fit value of Γ_0, the physical meaning of which is only as deep as the accuracy of this restriction.

Combining eqs 20−27 yields general expressions for the F^n-dependent resonance Stark effects, similar to eq 7 in Part 2. For example,

$$\Delta A(\bar{\nu},F^2) = \mathrm{Im}\left\{\frac{\epsilon(\bar{\nu})^2W(\bar{\nu})^{(2)}}{2!} + \epsilon(\bar{\nu})^3[W(\bar{\nu})^{(1)}]^2\right\} \times (Ff\Delta\mu_{CT})^2C_{CT}^{2\omega}*b(\bar{\nu}) \tag{28a}$$

$$\Delta A(\bar{\nu},F^4) = \mathrm{Im}\left[\left(\epsilon^2\frac{W^{(4)}}{4!} + \epsilon^3\left[\left(\frac{W^{(2)}}{2!}\right)^2 + 2W^{(1)}\frac{W^{(3)}}{3!}\right] + \epsilon^4 3(W^{(1)})^2\frac{W^{(2)}}{2!} + \epsilon^5(W^{(1)})^4\right)\right](Ff\Delta\mu_{CT})^4C_{CT}^{4\omega}*b(\bar{\nu}) \tag{28b}$$

where

$$C_{CT}^{n\omega} = \frac{1}{(n+1)(n+3)}\left[(n+3) + \frac{n}{2}(3\cos^2\chi - 1)(3\cos^2\zeta_{CT} - 1)\right] \tag{29}$$

As discussed in Part 2, in cases where

$$\Delta\vec{\mu}_{ge} = \vec{\mu}_e - \vec{\mu}_g \tag{30}$$

is nonzero, that is, $\bar{\nu}_0$ depends on $\vec{F}$, eq 28 accurately describes the resonance Stark effect contribution to the total Stark effect when $\Delta\vec{\mu}_{CT}$ is replaced by

$$\Delta\vec{\mu}'_{CT} = \Delta\vec{\mu}_{CT} - \Delta\vec{\mu}_{ge} \tag{31}$$

Experimental Issues. Adding together each of the F^n-dependent pieces in eq 28 would yield a result equivalent to subtracting a field-off absorption spectrum from a field-on absorption spectrum, as in eq 8. However, it is preferable to modulate the external field sinusoidally at a frequency ω and to isolate the time-dependent changes in absorbance that occur at the second, fourth, sixth, etc. harmonics of this frequency using lock-in detection (the odd harmonics have zero signal for an isotropic sample, eq 25). These signals are then multiplied by 2^{n-1} to yield higher-order Stark (HOS) spectra, $\Delta A(n\omega,F)$.[20] Since in the HOS experiment the field is described by

$$F = F_0\cos(\omega t + \theta) \tag{32}$$

the F^n-dependent terms in eq 25 yield nonzero terms at

frequencies for all even harmonics of ω from zero to n. The weighting of each contribution is given by the expansion of $\cos^n(\omega t + \theta)$ in terms of order one. Thus, for example,

$$\Delta A(2\omega) = 2\left(\frac{1}{2}\Delta A(F^2) + \frac{1}{2}\Delta A(F^4) + \frac{15}{32}\Delta A(F^6) + ...\right)$$
$$\Delta A(4\omega) = 8\left(\frac{1}{8}\Delta A(F^4) + \frac{3}{16}\Delta A(F^6) + \frac{7}{32}\Delta A(F^8) + ...\right) \quad (33)$$
$$\Delta A(6\omega) = 32\left(\frac{1}{32}\Delta A(F^6) + \frac{1}{32}\Delta A(F^8) + \frac{45}{512}\Delta A(F^{10}) + ...\right)$$

The relative importance of these terms clearly depends on the size of the field applied.

The HOS method was first applied to classical Stark effects where, for example, the contribution from $\Delta A(F^6)$ to $\Delta A(4\omega)$ was less than a few percent of the contribution from $\Delta A(F^4)$. Thus one could treat $\Delta A(4\omega)$ as an F^4-dependent spectrum without introducing much error. However, as suggested by the sizes of the HOS spectra in Parts 1 and 2, resonance Stark effects can be so large that these terms are not at all negligible for a 1 MV/cm field. In Parts 1 and 2, this complication due to lock-in detection was not ignored, but it was not dealt with properly. The contribution of $\Delta A(F^6)$ to $\Delta A(4\omega)$ was successfully removed by subtracting the appropriate weight of $\Delta A(6\omega)$ (from eq 33); however, this method failed to eliminate a substantial contribution from $\Delta A(F^8)$ to $\Delta A(4\omega)$. Moreover, since no $\Delta A(8\omega)$ spectra were acquired, no similar correction was applied to $\Delta A(6\omega)$.

There is an important side note to this phenomenon. To standardize the reporting of Stark spectra, we typically scale all spectra to 1 MV/cm assuming that $\Delta A(n\omega)$ is equal to $\Delta A(F^n)$. In the plots shown for resonance Stark effects, we continue to scale spectra to 1 MV/cm as if this assumption applied, but the fitting procedure for all resonance Stark spectra is carried out using the actual value of the field as applied in the experiment. This procedure is an effective compromise between the desire to make published Stark spectra readily comparable and the necessity of fitting to the precise value of electric field with which the data were acquired.

Results and Analysis

The Form of $V(\bar{\nu})$. We need not assume the Condon approximation or other assumptions about $V(\bar{\nu})$ to make the general result from combining eqs 28 and 33 applicable to the analysis of HOS spectra. ζ_{CT} is the only factor that contributes to the variation in the HOS spectra with χ; thus, its determination is straightforward if χ can be varied experimentally.[21] If HOS spectra can also be obtained for just two values of n, the distinct contributions of $\Delta\mu_{CT}$ and $V(\bar{\nu})$ to the line shapes and amplitudes of these spectra can be revealed through simulations. The determination of $V(\bar{\nu})$ in this manner then provides opportunities to identify the physical model that gives rise to $V(\bar{\nu})$.

If instead we do assume the Condon approximation and consider only the couplings between the ground vibrational state of the ψ_e surface and an effective continuum of vibrational states on the ψ_{CT} surface, we are led, as described above, to consider either Gaussian (if $k_BT \gg \bar{\nu}_{mean}$) or Pekarian (if $k_BT \ll \bar{\nu}_{mean}$) forms for $\rho_{FC}(\bar{\nu})$ and thus for $|V(\bar{\nu})|^2$. Figure 2 compares the 6th and 12th derivatives of normalized Gaussian (dashed) and Pekarian (solid) distributions plotted against a reduced coordinate, $\xi = (\bar{\nu} - \bar{\nu}_{CT})/\Delta_{CT}$; $\bar{\nu}_{CT}$ is the frequency where each achieves its maximum, and Δ_{CT} is the full width at half-maximum (fwhm) of each curve.[22] Plotting these curves in this way highlights their difference in skewness and higher moments; the Pekarian, $P(\bar{\nu})$, often referred to as a Poisson distribution, is slightly narrower than the Gaussian, $G(\bar{\nu})$, to negative values of ξ and is slightly wider to positive values. With increasing derivative order, the derivatives of $P(\bar{\nu})$ get steadily larger than those of $G(\bar{\nu})$ for negative ξ and smaller for positive ξ. There is also a significant shift of the zero crossings of the derivatives of $P(\bar{\nu})$ toward negative ξ. These observations apply to the Hilbert transforms of these functions as well (not shown).

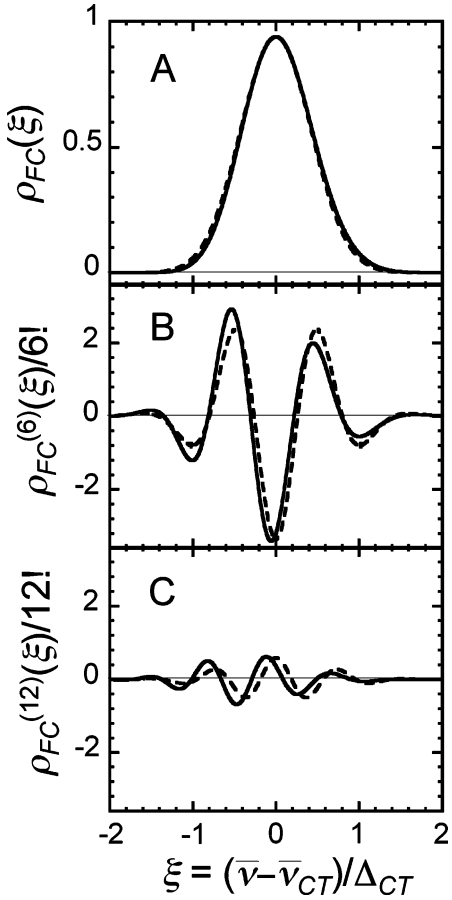

Figure 2. A normalized Pekarian (solid), Gaussian (dashed), and their derivatives. Plotting these functions against the reduced coordinate ξ is equivalent to setting equal their positions of maximum amplitude, $\bar{\nu}_{CT}$, and their full widths at half-maximum, Δ_{CT}.

These differences can affect analyses of HOS spectra (eq 28) and estimations of rates based on these analyses (eq 6). Figure 3 illustrates how the substitution of $G(\bar{\nu})$ for $P(\bar{\nu})$ can affect simulated HOS spectra using the fit to the absorption spectrum and the resonance Stark effect of the B_L band in M203GD mutant of bacterial RCs, as described in Part 4 of this series; using $\Delta_{CT} = 1000$ cm^{-1} and $\bar{\nu}_{CT} = 12\,870$ cm^{-1} for these simulations, the region between $\bar{\nu} = 12\,000$ and $13\,000$ cm^{-1} plotted in Figure 3 corresponds to the region between $\xi = -0.87$ and 0.13 in Figure 2. The different amplitudes of the HOS simulations calculated using $P(\bar{\nu})$ (black) and $G(\bar{\nu})$ (red) can thus be readily traced to the generally larger values of the derivatives of $P(\bar{\nu})$ in this vicinity. The shift of $\Delta A(6\omega)$ calculated using $G(\bar{\nu})$ with respect to $\Delta A(6\omega)$ calculated using $P(\bar{\nu})$ can also be traced to Figure 2, being caused by the shift between the derivatives.

As described above, the use of the Pekarian is consistent with a physical model for excited-state charge transfer in which (i) there is no horizontal displacement between the ground- and excited-state surfaces, (ii) the Condon approximation is valid, (iii) many normal vibrational modes are linearly electron−

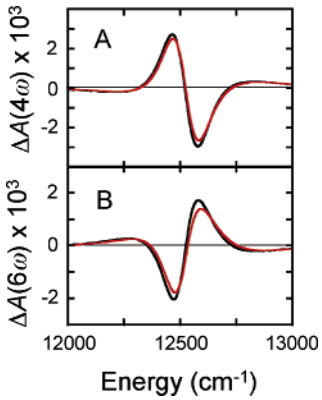

Figure 3. Resonance Stark effects depend on the form of $\rho_{FC}(\bar{\nu})$. The black and red curves were calculated using Pekarian and Gaussian forms, respectively. In both cases, $F = 0.67$ MV/cm, $\chi = 90°$, $\Delta_{CT} = 1000$ cm^{-1}, $W_R = 1.3$ cm^{-1}, $\delta = -0.34$, $f\Delta\mu_R = 1.06$ cm/MV, $\zeta_{CT} = 45°$, $\bar{\nu}_0 = 12\,530$ cm^{-1}, $\Gamma_0 = 90$ cm^{-1}, $\Gamma_{Gaus} = 50$ cm^{-1}, and the absorption peak height is 0.22. $\Delta A(4\omega)$ and $\Delta A(6\omega)$ spectra are scaled to an applied field of 1.0 MV/cm by dividing them by F^4 and F^6, respectively.

phonon coupled with small displacements, (iv) these many modes can be described by a mean frequency, $\bar{\nu}_{mean}$, and (v) $\bar{\nu}_{mean}$ is larger than the thermal energy available at 77 K. Because this thermal energy, only 54 cm^{-1}, is smaller than the energies of most intramolecular vibrations and many collective supramolecular modes and because fit quality is consistently better using $P(\bar{\nu})$ to fit resonance Stark effects associated with the B_L band in bacterial RCs,[4] we choose to use $P(\bar{\nu})$ as the basis for other calculations below; nevertheless, the accompanying conclusions are the same whether a normalized Gaussian or a normalized Pekarian is used for $\rho_{FC}(\bar{\nu})$.

Fitting Spectra: Definition of Fit Quality and Covariances among Resonance Stark Parameters. Because resonance Stark spectroscopy promises to provide information on parameters that affect rates of charge transfer that have not been available before in most cases, it is important to understand the process used to extract parameters and pitfalls that may result. We have suggested that, within this model, resonance Stark effects depend on parameters controlled by experiment (n,F,χ), parameters from radiationless transition theory (V_0,$\bar{\nu}_{CT}$,Δ_{CT}), parameters that describe the distance and direction of charge separation ($\Delta\mu_{CT}$,ζ_{CT}), and parameters that describe the absorption spectrum in the absence of the applied field ($\bar{\nu}_0$,Γ_0,Γ_{Gaus}).[23] No two of these parameters are completely orthogonal, yet of all of these parameters only two pairs have identical effects on $\Delta A(n\omega)$: these pairs are F and $\Delta\mu_{CT}$ and χ and ζ_{CT}. Fortunately, both F and χ are experimental parameters, which can be quantified separately from an analysis of the HOS spectra.[24] Similarly, the parameters with which the absorption spectra are fit might be determined separately from an analysis of the HOS spectra, reducing the number of unknowns with which the resonance Stark effects are fit to five: V_0, $\bar{\nu}_{CT}$, Δ_{CT}, $\Delta\mu_{CT}$, and ζ_{CT}.

The contributions of these five parameters can be separated by collecting Stark spectra for multiple values of χ and n. First, ζ_{CT} alone affects the HOS spectra obtained as a function of χ. Second, whereas the weighting of each term in the determination of $\Delta A(\bar{\nu},F^n)$ depends identically upon $\Delta\mu_{CT}$, many of those contributions have differing dependences upon V_0. Third, the line shape of each of these terms is influenced differently by the relative positions of the maxima of Im[$\epsilon(\bar{\nu})$] and $V(\bar{\nu})$, $\bar{\nu}_0 - \bar{\nu}_{CT}$, as by their relative widths, $(\Gamma_0 + \Gamma_{et})/\Delta_{CT}$. These distinctions among the effects of these parameters upon the HOS spectra are what make them separable.

When data are fit, two questions arise: (i) how does one define the best fit, and (ii) what are the covariances among the fit parameters? With regard to the first question, one might want to weight differently the residuals from different $\Delta A(n\omega)$. For example, overlapping signals due to classical Stark effects should distort RSEs to a lesser extent as n increases.[3] In contrast, if there are deviations of either $\epsilon(\bar{\nu})$ or $V(\bar{\nu})$ from the line shapes that are imposed in the analysis, the effects of those deviations should become increasingly important with increasing n. Also, as is evident from Figure 7 below, RSEs can have significant features over a much broader region of the spectrum than that defined by the fwhm of the absorption band. Thus, judging fit quality by the sum of the squared residuals across the entire spectrum may give too much weight to the features on the wings of the HOS spectra in the case that there are overlapping Stark effects there due to other bands. With these considerations in mind, for the fits here and in Part 4, we choose to confine the sum of the squared residuals to a region within 500 cm^{-1} to either side of $\bar{\nu}_0$ and to weight the residuals from the 4ω and 6ω spectra identically.

With regard to the second question above, substantial covariances between some of these parameters do arise. In particular, if the value of Δ_{CT} cannot be obtained precisely from a fit to the HOS spectra, then the values of V_0^2, $\Delta\mu_{CT}$, and $\bar{\nu}_0 - \bar{\nu}_{CT}$ are at least as uncertain as Δ_{CT}. The reasons for this are most easily demonstrated using a Gaussian form for $|V(\bar{\nu}_0)|^2$:

$$|V(\bar{\nu}_0)|^2 = 2\left[\frac{\ln 2}{\pi}\right]^{1/2}\frac{V_0^{\,2}}{\Delta_{CT}}\exp\left[-4\ln 2\left(\frac{\bar{\nu}_0 - \bar{\nu}_{CT}}{\Delta_{CT}}\right)^2\right] \quad (34)$$

$|V(\bar{\nu})|^2$ is evaluated at $\bar{\nu}_0$ for this demonstration to provide a reference energy for the effect of the field on $|V(\bar{\nu})|^2$ generally. The change in $|V(\bar{\nu}_0)|^2$ for a donor−acceptor system due to the applied field is a product of (i) the factor $2[\ln 2/\pi]^{1/2}(V_0^2/\Delta_{CT})$ and (ii) the change in the value of the above exponential when $\bar{\nu}_{CT}$ is altered by the interaction of $\Delta\mu_{CT}$ with the field. This second term can be considered as a product of the value of this exponential in the absence of the field and the percentage change in this exponential due to the field. As evident from eqs 7 and 34, the percentage change in this exponential due to the field depends not only upon $\Delta\mu_{CT}$ but also upon Δ_{CT}; specifically, it depends on the ratio of these two parameters. Similarly the evaluation of this exponential in the absence of the field depends on the ratio of $\bar{\nu}_0 - \bar{\nu}_{CT}$ to Δ_{CT}. Taken together, the contributions to the HOS spectra from V_0^2, $\Delta\mu_{CT}$, and $\bar{\nu}_0 - \bar{\nu}_{CT}$, although separable from each other, are themselves inseparable from a factor of $1/\Delta_{CT}$.

Even though the covariances are substantial between these parameters and Δ_{CT}, the previous paragraph suggests that the covariances may be small between Δ_{CT} and either

$$W_R = V_0^{\,2}/\Delta_{CT} \quad (35)$$

$$\Delta\vec{\mu}_R = \Delta\vec{\mu}_{CT}/\Delta_{CT} \quad (36)$$

or

$$\delta = (\bar{\nu}_0 - \bar{\nu}_{CT})/\Delta_{CT} \quad (37)$$

Whereas $\Delta\mu_R$ and δ are the same reduced dipole moment and energy, respectively, that were introduced in Part 2 to simplify equations analgous to eq 28 above, Part 2 introduced a reduced coupling, denoted R and equal to V_0/Δ_{CT}, which is not the same reduced coupling as that defined by eq 35. W_R, discussed in Part 2 as $\Delta_{CT}R^2$, is preferred to R because fit values of W_R can

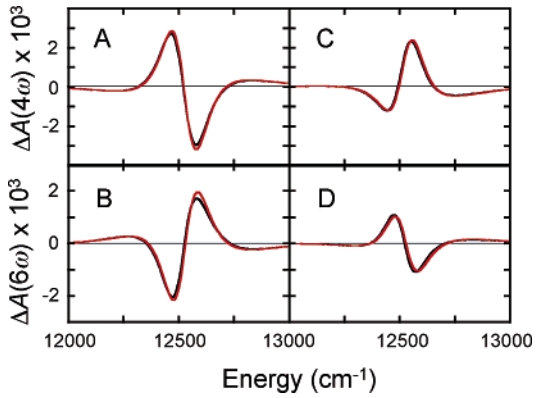

Figure 4. Resonance Stark effects are almost linearly proportional to W_R. The black curves in panels A and B are the same as the black curves in Figure 3. The black curves in panels C and D were calculated using $F = 0.64$ MV/cm and $\{W_R,\Delta\mu_R,\delta\} = \{1.2\ \text{cm}^{-1}, 1.08\ \text{cm/MV}, -0.41\}$; other details are the same as for the black curves in panels A and B. The corresponding red curves were calculated using the same values of all parameters except W_R. For the red curves W_R was divided by 2, and the resulting spectra were multiplied by 2 to aid comparison.

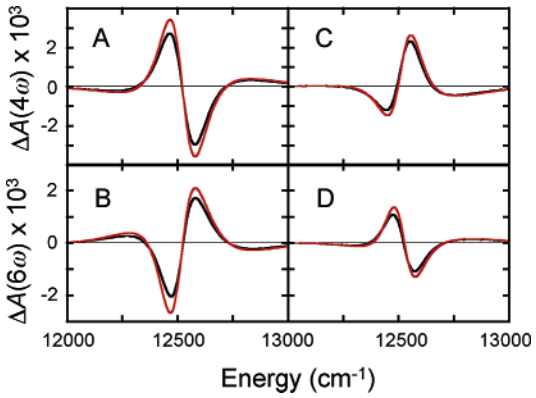

Figure 5. Resonance Stark effects are almost proportional to the nth power of $\Delta\mu_R$. The black curves in each panel are the same as those in Figure 4. The corresponding red curves were calculated using the same values of all parameters except $\Delta\mu_R$. For the red curves, $\Delta\mu_R$ was divided by $\sqrt{2}$, and the resulting $\Delta A(4\omega)$ and $\Delta A(6\omega)$ spectra were multiplied by 4 and 8 to aid comparison.

be shown to have the smaller covariance with fit values of Δ_{CT}. As demonstrated in Part 2, when HOS spectra are considered as a function of Δ_{CT}, $\Delta_{CT}R^2$, $\Delta\mu_R$, and δ, the effect of increasing Δ_{CT} when the other parameters are held constant is primarily to decrease the sharpness of the features at the shoulders and wings of the HOS spectra. The features at the center of the HOS spectra, both their line shapes and amplitudes, are nearly unaffected by changing Δ_{CT}. Thus, if these features at the center could be used to determine W_R, $\Delta\mu_R$, and δ uniquely, the covariances among these parameters and Δ_{CT} would indeed be small. The uniqueness of a fit to these features using W_R, $\Delta\mu_R$, and δ was demonstrated in Part 2, though it was not discussed in exactly these terms. We revisit some aspects of that demonstration here to estimate the covariances among these three terms.

Figure 4 illustrates that $\Delta A(4\omega)$ and $\Delta A(6\omega)$ are roughly linearly proportional to the value of W_R. The black spectra in panels A and B were calculated using the fit to the absorption spectrum and the resonance Stark effect of the B_L band in the M203GD mutant of bacterial RCs ($\delta = -0.34$); the black spectra in panels C and D were calculated using the fit for the Q_A^- preparation of this mutant ($\delta = -0.88$) (see Part 4). In each case, the red spectra are calculated for a value of W_R that is one-half that of the value used for the corresponding black spectra; the red spectra have additionally been multiplied by 2 to aid comparison.

Figure 5 illustrates that $\Delta A(n\omega)$ is roughly proportional to the nth power of $\Delta\mu_R$. The black spectra are the same as those in Figure 4. The red spectra in this case were calculated for a value of $\Delta\mu_R$ that is a factor of $\sqrt{2}$ smaller than the value used to calculate the corresponding black spectra; the red $\Delta A(4\omega)$ and $\Delta A(6\omega)$ have additionally been multiplied by 4 and 8, respectively, to aid comparison. The differences between these spectra are larger than those between the spectra where W_R was altered; nevertheless, the scaled red $\Delta A(n\omega)$ are similar to the black spectra within a factor of $\sqrt{2}$ over much of the spectrum. Such deviations from strict proportionality are less severe for smaller percentage changes in $\Delta\mu_R$.

These dependences of $\Delta A(n\omega)$ upon the first power of W_R and the nth power of $\Delta\mu_R$ make it straightforward to quantify the covariance between these parameters when multiple $\Delta A(n\omega)$ are fit simultaneously.[25] For example, if W_R is increased by 20%, these relationships suggest that $\Delta\mu_R$ must be decreased by 5% to recapture the original $\Delta A(4\omega)$; however, $\Delta A(6\omega)$ will now be 10% smaller than it was originally. Similarly, a 3% decrease in $\Delta\mu_R$ may recapture the original $\Delta A(6\omega)$, but $\Delta A(4\omega)$ will now be 7% too large. Thus, if for any reason W_R is uncertain by 20%, $\Delta\mu_R$ is uncertain by roughly 4%.

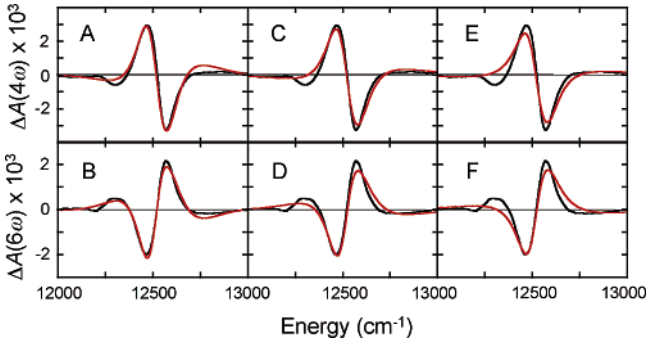

Figure 6. Fits (red curves) to the resonance Stark effect of the B_L band in M203GD RCs (black curves) as a function of Δ_{CT}. Best fits for $\Delta_{CT} = 700\ \text{cm}^{-1}$ (panels A and B), $1000\ \text{cm}^{-1}$ (panels C and D), and $1500\ \text{cm}^{-1}$ (panels E and F) use $\{W_R,\Delta\mu_R,\delta\}$ equal to $\{1.4\ \text{cm}^{-1}, 1.06\ \text{cm/MV}, -0.32\}$, $\{1.3\ \text{cm}^{-1}, 1.06\ \text{cm/MV}, -0.34\}$, and $\{1.1\ \text{cm}^{-1}, 1.09\ \text{cm/MV}, -0.33\}$, respectively. Other details of the calculations are the same as for the black curves in Figure 3.

The HOS line shapes in Figures 4 and 5 change only slightly as the values of W_R and $\Delta\mu_R$ are changed. Thus the value of δ is indeed the principal determinant of line shape, and its fit value is nearly independent of W_R and $\Delta\mu_R$ in the range in which these parameters may be changed without significantly affecting the fit quality.

We conclude this discussion of the covariances among the resonance Stark parameters with a practical example. Figure 6 shows the best fits to the resonance Stark effect of the B_L band in RCs with the M203GD mutation (see Part 4) when Δ_{CT} equals $700\ \text{cm}^{-1}$ (panels A and B), $1000\ \text{cm}^{-1}$ (panels C and D), or $1500\ \text{cm}^{-1}$ (panels E and F); in each case, the values of W_R, $\Delta\mu_R$, and δ are varied while other parameters are held constant. Fit quality was judged by the sum of the squared residuals calculated over a window of $\pm 500\ \text{cm}^{-1}$ around $\bar{\nu}_0$ with the residuals from $\Delta A(4\omega)$ and $\Delta A(6\omega)$ weighted evenly. This sum was calculated for a large grid of parameter sets $\{W_R,\Delta\mu_R,\delta\}$, where W_R was incremented by roughly 2% of its fit value, $\Delta\mu_R$ was incremented by roughly 1% of its fit value, and δ was incremented by 0.01 units. Whereas the fit using $700\ \text{cm}^{-1}$ for Δ_{CT} most closely captures the principal features of the observed

$\Delta A(4\omega)$ and $\Delta A(6\omega)$, the fit using 1000 cm^{-1} is slightly broader than the observed spectra, and the fit using 1500 cm^{-1} is broader still. Nevertheless, the best fit sets $\{W_R,\Delta\mu_R,\delta\}$ using Δ_{CT} equal to 700, 1000, and 1500 cm^{-1} are quite similar: they are {1.4 cm^{-1},1.06 cm/MV,−0.32}, {1.3 cm^{-1},1.06 cm/MV,−0.34}, and {1.1 cm^{-1},1.09 cm/MV,−0.33}, respectively. Thus these reduced parameters can be well determined, even if the value of Δ_{CT} is difficult to determine from the fit.

Utilizing a Gaussian form for $\rho_{FC}(\bar{\nu})$ in eq 6, k_{et} can be rewritten as a function of only these reduced parameters,

$$k_{et} = 4[\pi^3 \ln 2]^{1/2} W_R \exp[-4 \ln 2 \cdot \delta^2] \qquad (38)$$

Thus k_{et} can also be well determined in the absence of a well determined value for Δ_{CT}. However, as suggested by Figure 3A, different forms for $\rho_{FC}(\bar{\nu})$ can lead to different predicted rates for the same values of W_R and δ. If either Gaussian or Pekarian forms for $\rho_{FC}(\bar{\nu})$ are used, the predicted rates should be quite similar within a standard deviation of $\delta = 0$, but their relative values may be considerably different at multiple standard deviations from the mean.

Fitting Spectra: Covariances among Absorption and Resonance Stark Parameters. In the case of the coupling between B_L^* and $B_L^+H_L^-$ in the bacterial RC, the resonance Stark analysis is complicated by the spectral overlap between the $B_L^* \leftarrow B_L$ transition and other transitions (this would likely be much less of a problem for synthetic charge-transfer systems). This spectral overlap compromises the precision with which the amplitude, position, and line shape of this transition are known. Here we assess the covariances that appear generally between these absorption parameters and the resonance Stark parameters.

To begin with, an underestimation by 10% of the peak amplitude of the absorption translates to an overestimation by 10% of the amplitudes of all $\Delta A(n\omega)$ relative to the absorption. As we demonstrated above, every $\Delta A(n\omega)$ depends roughly linearly upon W_R and as the nth power of $\Delta\mu_R$. Thus this factor of 10% should result in an overestimation of the value of W_R by close to 10%; any relative change in the fit value of $\Delta\mu_R$ should be much smaller than this. An overestimation of W_R by 10% corresponds to a roughly 5% overestimation of V_0.

According to eq 28, homogeneous broadening and inhomogeneous broadening enter the calculation of HOS spectra in distinct ways: whereas powers of the homogeneous line shape are entangled with derivatives of $\rho_{FC}(\bar{\nu})$, the inhomogeneous broadening $b(\bar{\nu})$ affects $\Delta A(n\omega)$ in the same manner as it affects absorption. Nevertheless, for the accurate analysis of resonance Stark effects it is more important to determine the overall line width of an absorption band than to determine the separate contributions of homogeneous and inhomogeneous broadening to its line shape. This conclusion can be drawn from Figure 7, where the black curves from Figure 4 ($\Gamma_0 = 90$ cm^{-1}, $\Gamma_{Gaus} = 50$ cm^{-1}) are plotted against simulations where either Γ_0 has been increased to 110 cm^{-1} (red) or Γ_{Gaus} has been increased to 90 cm^{-1} (blue). Both modifications increase the fwhm of the absorption bands (panels A and D) by almost 20%. As evident from the simulations of the HOS spectra, these perturbations to the absorption line shape affect the resonance Stark effects nearly identically. Thus, for reasonable errors in the apportionment of an absorption line width to homogeneous and inhomogeneous contributions, there should not be significant differences in the fit values of W_R, $\Delta\mu_R$, and δ.

Interestingly, fit quality is quite sensitive to the value of $\bar{\nu}_0$, although the fit values of W_R and $\Delta\mu_R$ are not. This is illustrated in Figure 8, where we show the best fits to the resonance Stark effects of the B_L band in M203GD RCs upon setting $\bar{\nu}_0$ to either 12 510 cm^{-1} (panels A and B), 12 530 cm^{-1} (panels C and D), or 12 550 cm^{-1} (panels E and F). The best fit sets $\{W_R,\Delta\mu_R,\delta\}$ for these spectra are {1.2 cm^{-1},1.08 cm/MV,−0.41}, {1.3 cm^{-1},1.06 cm/MV,−0.34}, and {1.4 cm^{-1},1.04 cm/MV,−0.26}, respectively. As one might expect, since both W_R and $\Delta\mu_R$ have been shown to affect line shapes only weakly, the shifts in $\bar{\nu}_0$ are compensated primarily by adjustments to the fit values of δ.

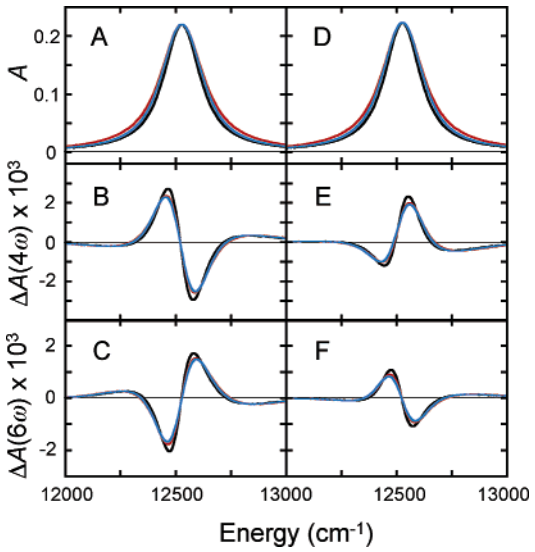

Figure 7. Analogous perturbations to the values of Γ_0 and Γ_{Gaus} affect resonance Stark effects similarly. The black curves in panels B, C, E, and F are the same as those in Figure 4, panels A, B, C and D, respectively ($\Gamma_0 = 90$ cm^{-1} and $\Gamma_{Gaus} = 50$ cm^{-1}). The red curves correspond to $\Gamma_0 = 110$ cm^{-1} and $\Gamma_{Gaus} = 50$ cm^{-1}. The blue curves correspond to $\Gamma_0 = 90$ cm^{-1} and $\Gamma_{Gaus} = 90$ cm^{-1}. Panels A and D illustrate the corresponding absporption spectra.

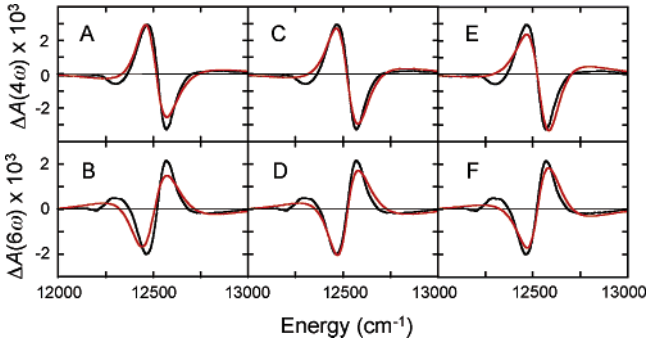

Figure 8. Fits (red curves) to the resonance Stark effect of the B_L band in M203GD RCs (black curves) as a function of $\bar{\nu}_0$. Best fits for $\bar{\nu}_0 = 12\,510$ cm^{-1} (panels A and B), 12 530 cm^{-1} (panels C and D), and 12 550 cm^{-1} (panels E and F) use $\{W_R,\Delta\mu_R,\delta\}$ equal to {1.2 cm^{-1},1.08 cm/MV,−0.41}, {1.3 cm^{-1},1.06 cm/MV,−0.34}, and {1.4 cm^{-1},1.04 cm/MV,−0.26}, respectively. Other details of the calculations are the same as for the black curves in Figure 3.

Relationship of the Resonance Stark Parameters to Marcus Parameters. As described in the Introduction, the simplest electron-transfer theories attempt to simplify the description of the initial and final state potential energy surfaces to two parameters, $\Delta\bar{\nu}$ and λ, often called Marcus parameters. This minimal description hinges upon the assumption that both the initial and final state potential energy surfaces are parabolic with the same $\bar{\nu}_{mean}$. As long as $\bar{\nu}_{mean}$ is the same for both surfaces, one can uniquely determine the energy of the transition state from $\Delta\bar{\nu}$ and λ and hence the rate of electron transfer as well using eq 2. This equation neglects nuclear tunneling and

assumes that the populations of the vibrational levels on the initial-state surface are at equilibrium.

Similarly, the radiationless transition picture of electron transfer provides eq 38 for evaluating a rate constant from just two parameters describing the reaction surface geometry, δ and Δ_{CT}, which is embedded in the factor W_R. This calculation also hinges upon the assumption that both the initial- and final-state surfaces have the same $\bar{\nu}_{mean}$. Although the differences between eqs 2 and 38 reflect the important conceptual distinction that the radiationless transition has been assumed to occur exclusively by nuclear tunneling from the lowest vibrational level of the reactant state, they are nevertheless united by the similarities illustrated in Figure 1. Transforming δ and Δ_{CT} into $\Delta\bar{\nu}$ and λ is not straightforward, however, so we will outline the transformation here.

The parameter $\bar{\nu}_{mean}$ is related to λ by the Huang−Rhys parameter (eq 16):

$$\lambda = \bar{\nu}_{mean} \cdot S \tag{39}$$

Since the standard deviation of the Pekarian, σ, is given by[19]

$$\sigma = \bar{\nu}_{mean}\sqrt{S} \tag{40}$$

and the fwhm of the Pekarian, Δ_{CT}, is related to σ by[19]

$$\Delta_{CT} = \sigma\sqrt{5.57} \tag{41}$$

($\Delta_{CT} = \sigma\sqrt{5.545}$ for a Gaussian), we get the following relationship between λ, $\bar{\nu}_{mean}$, and Δ_{CT}:

$$\lambda = \frac{{\Delta_{CT}}^2}{5.57\bar{\nu}_{mean}} \tag{42}$$

Referring to Figure 1, once λ is known, $\Delta\bar{\nu}$ can be calculated from δ and Δ_{CT} according to

$$\Delta\bar{\nu} = \delta \cdot \Delta_{CT} + \lambda \tag{43}$$

Thus we have demonstrated that one needs a value for $\bar{\nu}_{mean}$ to discuss resonance Stark fit parameters in terms familiar to the bulk of the electron-transfer literature. Either description is sufficient for the calculation of a rate constant, but one cannot navigate between the two without this additional information.

Acknowledgment. T.P.T. is supported by a predoctoral fellowship from the Fannie and John Hertz Foundation and a Stanford Graduate Fellowship. This work was supported by grants from the NSF Biophysics and Chemistry Divisions.

References and Notes

(1) Zhou, H. L.; Boxer, S. G. *J. Phys. Chem. B* **1998**, *102*, 9139.
(2) Bublitz, G. U.; Boxer, S. G. *Annu. Rev. Phys. Chem.* **1997**, *48*, 213.
(3) Zhou, H. L.; Boxer, S. G. *J. Phys. Chem. B* **1998**, *102*, 9148.
(4) Treynor, T. P.; Ishii, C. Y.; Boxer, S. G. *J. Phys. Chem. B* **2004**, *108*, 13523.
(5) Marcus, R. A.; Sutin, N. *Biochim. Biophys. Acta* **1985**, *811*, 265.
(6) For compactness, we have adopted the following notation conventions: (i) if a symbol is used in both subscripted and unsubscripted forms, then the unsubscripted symbol refers to the general class of the subscripted symbols; (ii) if a symbol such as m is used as both m and $\vec{m}$, then m alone refers to the norm of $\vec{m}$, $|\vec{m}\cdot\vec{m}|^{1/2}$; (iii) if a symbol such as $\Delta\bar{\nu}$ is used as both $\Delta\bar{\nu}$ and $\Delta\bar{\nu}(F)$, then $\Delta\bar{\nu}$ alone refers to the F-independent component of $\Delta\bar{\nu}(F)$.
(7) Marcus, R. A. *J. Chem. Phys.* **1956**, *24*, 966.
(8) Hush, N. S. *Prog. Inorg. Chem.* **1967**, *8*, 391.
(9) Treynor, T. P.; Boxer, S. G. *J. Phys. Chem. A* **2004**, *108*, 1764.
(10) Treynor, T. P.; Andrews, S. S.; Boxer, S. G. *J. Phys. Chem. B* **2003**, *107*, 11230.
(11) Robinson, G. W.; Frosch, R. P. *J. Chem. Phys.* **1962**, *37*, 1962.
(12) Fano, U. *Phys. Rev.* **1961**, *124*, 1866.
(13) Zhou, H. L.; Boxer, S. G. *J. Phys. Chem. B* **1997**, *101*, 5759.
(14) Brunschwig, B. S.; Creutz, C.; Sutin, N. *Coord. Chem. Rev.* **1998**, *177*, 61.
(15) Liptay, W. *Angew. Chem., Int. Ed. Engl.* **1969**, *8*, 177.
(16) Liptay, W. In *Excited States*; Lim, E. C., Ed.; Academic: New York, 1974; Vol. 1, p 129.
(17) Huang, K.; Rhys, A. *Proc. R. Soc. London, Ser. A* **1950**, *204*, 406.
(18) Sturge, M. D.; Guggenheim, H. J.; Pryce, M. H. L. *Phys. Rev. B: Solid State* **1970**, *2*, 2459.
(19) Markham, J. J. *Rev. Mod. Phys.* **1959**, *31*, 956.
(20) Lao, K.; Moore, L. J.; Zhou, H. L.; Boxer, S. G. *J. Phys. Chem.* **1995**, *99*, 496.
(21) If the extra terms in eq 33 make significant contributions, there will be a tendency to overestimate ζ_{CT} slightly from the ratios of the Stark spectra when $\chi = 90°$ and $\chi \neq 90°$. If the planes of the slides sandwiching the sample are not exactly parallel, this imperfection will introduce error into the determination of χ from the ratio of the absorbances of the sample when $\chi = 90°$ and $\chi \neq 90°$.
(22) The plots of the normalized Gaussian and its derivatives in Figure 4 of Part 2 were multiplied by an additional factor of π that was not mentioned in the figure caption.
(23) RSEs also depend on the value of f, which we assume is equal to 1.0 in the following discussion.
(24) F depends on the sample thickness, which we determine from the index of refraction and fringe spacing in the absorption spectra of our Stark samples. Both can be measured with high accuracy if the planes of the slides sandwiching the sample are truly parallel. If the slides are in fact skewed or bowed, these qualities will introduce errors that propagate primarily into the determination of $\Delta\mu_{CT}$ and ζ_{CT}.
(25) These conclusions were supported by an analysis of eq 7 in Part 2 in a limit where $W_R \ll \Gamma_0$; however, this is not a sufficient condition to ignore all the other terms in this equation since they can be quite significant when added together. Additionally we have demonstrated in this paper the importance of including $\Delta A(F^6)$ and other terms in the calculation of $\Delta A(4\omega)$.